Available online at www.sciencedirect.com
ScienceDirect
Journal of Power Sources 173 (2007) 495–501
JOURNAL OF POWER SOURCES
www.elsevier.com/locate/jpowsour

Lithium recycling behaviour of nano-phase-$CuCo_2O_4$ as anode for lithium-ion batteries

Yogesh Sharma, N. Sharma, G.V. Subba Rao, B.V.R. Chowdari *

Department of Physics, National University of Singapore, Singapore 117542, Singapore

Received 27 March 2007; received in revised form 5 June 2007; accepted 7 June 2007
Available online 19 June 2007

Abstract

Nano-$CuCo_2O_4$ is synthesized by the low-temperature (400 °C) and cost-effective urea combustion method. X-ray diffraction (XRD), high resolution transmission electron microscopy (HR-TEM) and selected area electron diffraction (SAED) studies establish that the compound possesses a spinel structure and nano-particle morphology (particle size (10–20 nm)). A slight amount of CuO is found as an impurity. Galvanostatic cycling of $CuCo_2O_4$ at 60 mA g^{-1} in the voltage range 0.005–3.0 V versus Li metal exhibits reversible cycling performance between 2 and 50 cycles with a small capacity fading of 2 mAh g^{-1} per cycle. Good rate capability is also found in the range 0.04–0.94*C*. Typical discharge and charge capacity values at the 20th cycle are 755(±10) mAh g^{-1} (∼6.9 mol of Li per mole of $CuCo_2O_4$) and 745(±10) mAh g^{-1} (∼6.8 mol of Li), respectively at a current of 60 mA g^{-1}. The average discharge and charge potentials are ∼1.2 and ∼2.1 V, respectively. The underlying reaction mechanism is the redox reaction: Co ↔ CoO ↔ Co_3O_4 and Cu ↔ CuO aided by Li_2O, after initial reaction with Li. The galvanostatic cycling studies are complemented by cyclic voltammetry (CV), ex situ TEM and SAED. The Li-cycling behaviour of nano-$CuCo_2O_4$ compares well with that of iso-structural nano-Co_3O_4 as reported in the literature.
© 2007 Published by Elsevier B.V.

Keywords: $CuCo_2O_4$; Spinel structure; Anode material; Rate capability; Li-ion batteries

1. Introduction

Binary and ternary transition metal oxides, especially those containing cobalt, are materials of interest as prospective anodes to replace graphite in present-day lithium-ion batteries (LIBs) owing to the high reversible capacities obtainable with the optimized compositions and morphologies [1–12]. Nano-phase CoO [1,2], CoO–Li_2O composite [7] and Co_3O_4 [1,3–6] exhibit capacities in the range of 700–950 mAh g^{-1} in the voltage window 0.005–3.0 V and have been well studied. Co_3O_4 possesses a cubic inverse spinel structure. Due to the high cost and toxic nature of cobalt, it is highly desirable to replace it partially or fully with relatively inexpensive and eco-friendly metals and examine their lithium recyclability. Till now, only preliminary studies on $NiCo_2O_4$ [8] and $ZnCo_2O_4$ [10] possessing the spinel structure and derived from the parent Co_3O_4 by replacing one cobalt by Ni and Zn have been reported. Our recent study [11] has shown that nano-phase $ZnCo_2O_4$ exhibits a reversible capacity of ∼900 mAh g^{-1} and is stable up to 60 cycles in the voltage range 0.005–3.0 V. Further, it has been established [11] that the presence of the Co/Co-oxide redox couple has given improved cycling characteristics of Li–Zn alloy and that of ZnO [11].

Another mixed oxide with spinel structure that can be studied as a LIB anode is $CuCo_2O_4$. It contains less cobalt than Co_3O_4 and Cu is also electrochemically active by virtue of a conversion reaction ($Cu + Li_2O \leftrightarrow 2Li + CuO$). An earlier report [13] stated that the compound can be synthesized only under high-pressure and high-temperature conditions. Petrov et al. [14] and Tavares et al. [15] using low-temperature calcinations of the precursor metal nitrates were able to prepare the cubic-form of $CuCo_2O_4$ with almost full stoichiometry. CuO is expected to undergo electrochemical cycling with Li with change in the oxidation state of Cu from 0 (metal; formed upon deep discharge) to +1 or +2 valency during the charge cycle [12]. Similarly, cobalt also undergoes redox reaction from Co^0 (metal; formed upon deep discharge) to Co^{2+} or Co^{3+} in the charged state [1,3–6,11]. Thus, analogous to $ZnCo_2O_4$ [11], the discharge–charge reaction of $CuCo_2O_4$ with Li can be represented by Eqs. (1)–(4). We can

* Corresponding author. Tel.: +65 6516 2531; fax: +65 6777 6126.
E-mail address: phychowd@nus.edu.sg (B.V.R. Chowdari).

0378-7753/$ – see front matter © 2007 Published by Elsevier B.V.
doi:10.1016/j.jpowsour.2007.06.022

expect a reversible capacity corresponding to 6 mol of Li per mole of $CuCo_2O_4$ (Eqs. (2) and (3)) and, in the most favorable case with the contribution from Eq. (4), a capacity of 7.33 mol of Li.

$$Cu^{2+}Co^{3+}{}_2O_4 + 8Li^+ + 8e^- \rightarrow Cu + 2Co + 4Li_2O \quad (1)$$

$$Cu + Li_2O \leftrightarrow CuO + 2Li^+ + 2e^- \quad (2)$$

$$2Co + 2Li_2O \leftrightarrow 2CoO + 4Li^+ + 4e^- \quad (3)$$

$$2CoO + \tfrac{2}{3}Li_2O \leftrightarrow \tfrac{2}{3}Co_3O_4 + \tfrac{4}{3}Li + \tfrac{4}{3}e^- \quad (4)$$

In the present report, $CuCo_2O_4$ is prepared in a nano-phase form by employing the easy and cost-effective urea combustion method at a relatively low-temperature, viz., ~400 °C. Its lithium recyclability is examined. Results show that the performance of $CuCo_2O_4$ compares well with that of nano-Co_3O_4 reported in the literature in terms of reversible capacity, rate capability and potentials for the discharge and charge reactions. The data support the mechanism proposed in Eqs. (2)–(4).

2. Experimental

Nano-$CuCo_2O_4$ was prepared by a urea combustion method at 400 °C [11,16]. Stoichiometric amounts of CuO (0.032 mol; Merck) and $Co(OH)_2$ (0.064 mol; Aldrich) were dissolved separately in a minimum amount of concentrated HNO_3 (Merck) to obtain the respective nitrates. These solutions were then mixed and stirred at 50 °C for 1 h. Urea (0.192 mol; Fluka Chemika) was added and the solution heated at 80 °C for 12 h to evaporate the water slowly. The resulting powder was ground in an auto grinder and then calcined at 400 °C for 6 h in air, and then preserved in a desiccator.

Structural and morphological characterization was performed by taking X-ray diffraction (XRD) patterns using a Siemens D5005 diffractometer equipped with Cu Kα radiation and by transmission electron microscopy (TEM; JEOL JEM 3010 operating at 300 kV), respectively. The TEM images along with selected area electron diffraction (SAED) patterns have been recorded on the bare nano-$CuCo_2O_4$ powder and on the composite electrode recovered after 50 charge–discharge cycles. The doctor blade technique was used to prepare the composite electrode on an etched Cu-foil (thickness ~15 μm) for electrochemical cycling with the active material, Super P carbon and binder (Kynar 2801) in the weight ratio: 70:15:15. Lithium metal (Kyokuto Metal Co., Japan) foil was used as the counter electrode and a Celgard 2502 membrane as the separator. The electrolyte was $LiPF_6$ dissolved in ethylene carbonate (EC) and diethyl carbonate (DEC) (1:1 by volume, Merck Selectipur LP 40). The electrode and cell fabrication process have been described in our earlier report [9]. The composite electrode thickness is ~20 μm and the active mass of the $CuCo_2O_4$ is ~3 mg in a circular disc electrode of diameter ~16 mm.

The galvanostatic charge–discharge cycling and cyclic voltammetry were performed at room temperature (RT ~25 °C) by means of a computer-controlled, Bitrode multiple battery tester (model SCN, Bitrode, USA) and a Mac-pile II (Bio-logic France), respectively. The cells were aged for 24 h to attain an equilibrium condition and a stable open-circuit voltage (OCV) before testing. For ex situ TEM studies, the cell was charged to 3.0 V after 50 cycles and then dismantled in a glove box. The composite electrode containing the active material was recovered and washed thoroughly with DEC to remove the electrolyte. It was then dried inside the glove box and powder was scraped from the Cu foil. The recovered powder was ground and dispersed in ethanol using an ultrasonic miller (Transsonic 660/H Elma). A drop of the suspension was deposited on a carbon-coated Cu-grid and then dried under a table lamp for 15–20 min before transferring to the TEM vacuum chamber.

3. Results and discussion

3.1. Structural and morphological characterization

In the urea combustion method presently adopted for the synthesis of nano-$CuCo_2O_4$, the nitrate ions from the copper and cobalt nitrates act as the oxidizer and urea as the fuel, to evolve gases. The freshly formed metal oxides combine to give the ternary spinel compound at 400 °C. The excess urea in the reaction mixture also decomposes by reacting with oxygen from air to yield CO_2, N_2 and H_2O vapour [11]. These evolved gases inhibit the grain-growth of the freshly formed $CuCo_2O_4$ and thereby retain the nano-size nature of the particles. The as-prepared nano-$CuCo_2O_4$ is black, fluffy and voluminous.

The XRD pattern of $CuCo_2O_4$ is shown in Fig. 1. It shows peaks that match with the cubic spinel structure, along with a small amount of CuO as a secondary phase. These features are similar to those reported by Tavares et al. [15]. The cubic lattice parameter, evaluated by least-squares fitting of 2θ and ($h\,k\,l$), is $a = 8.129(4)$ Å. This is in good agreement with the value of 8.133(2) Å (JCPDS card no. #78-2177 and from Ref. [15]) and reveals the formation of a compound $Cu_xCo_{2-x}O_4$ ($x \geq 0.95$) in almost phase-pure form. The HR-TEM image in Fig. 2a shows that $CuCo_2O_4$ consists of agglomerates of nano-particles with a size of 15–20 nm. The high resolution lattice image in Fig. 2b confirms the crystalline nature of the compound with very clear sets of lattice planes. The inter-planer distances (*d*-

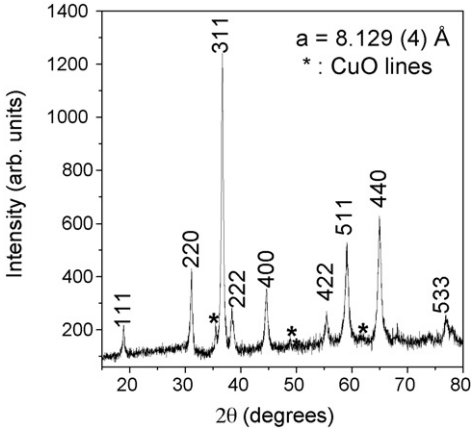

Fig. 1. Powder X-ray diffraction (XRD) pattern of nano-$CuCo_2O_4$. Miller indices ($h\,k\,l$) are shown. Cu Kα radiation. Asterisk indicates the lines due to impurity of CuO.

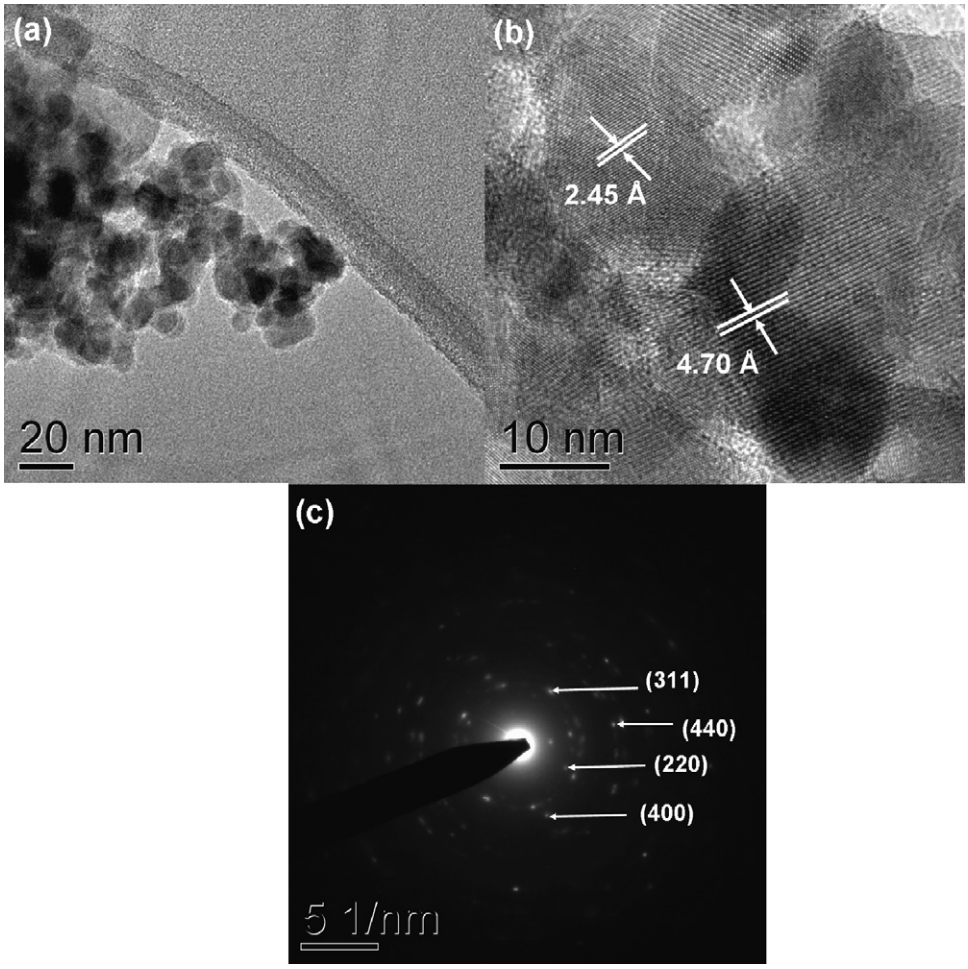

Fig. 2. (a) TEM photograph of $CuCo_2O_4$. (b) High resolution lattice image, showing well-defined nano-crystalline regions. (c) The SAED pattern showing diffuse spots and rings indicating nano-phase of $CuCo_2O_4$. The assigned Miller indices ($h\,k\,l$) to the marked spots are shown.

values) that correspond to some of the planes are 2.45 (±0.01) Å and 4.70 (±0.01) Å. These values are in good agreement with the *d*-spacings corresponding to the (3 1 1) and (1 1 1) planes, respectively, of the XRD pattern shown in Fig. 1. The SAED pattern in Fig. 2c comprises diffuse concentric rings with superimposed bright spots that are indicative of the-nano-crystalline nature of $CuCo_2O_4$. The $h\,k\,l$ (Miller indices) assigned from the *d*-spacings derived from the symmetrically spaced bright spots/ring diameters are indicated in Fig. 2c and match very well with those of the XRD pattern (Fig. 1).

3.2. Electrochemical properties

3.2.1. Galvanostatic cycling

In order to check the suitability of $CuCo_2O_4$ as a LIB anode, it was subjected to electrochemical cycling under galvanostatic conditions. Cycling was performed with half-cell configuration with $CuCo_2O_4$ as a cathode versus Li-metal in the voltage range 0.005–3.0 V at a current rate of 60 mA g^{-1}. The first discharge reaction commences cathodically from the OCV (∼2.8 V) to 0.005 V. The voltage profiles (voltage versus capacity curves) for selected cycles are shown in Fig. 3a and b. Fig. 3c presents the differential capacity (dq/dV) versus voltage plots corresponding to the 1st, 2nd and 10th cycles evaluated from the voltage versus capacity plots of Fig. 3a and b. The following conclusions can be drawn from the observed data. The first discharge reaction shows a large voltage plateau at ∼1.25 V followed by a sloping profile to the cut-off voltage, 0.005 V, with an overall discharge capacity of 1147 mAh g^{-1} (∼10.4 mol of Li per mole of $CuCo_2O_4$). The first charge curve shows a smoothly varying profile followed by a plateau at ∼2.1 V and the overall charge capacity is 828 mAh g^{-1} (∼7.6 mol of Li). The difference between the first discharge and charge capacity corresponds to an irreversible capacity loss (ICL) of ∼28% (319 mAh g^{-1}, ∼2.8 mol of Li).

The second discharge reaction, the profile of which is different from the first discharge reaction, shows a plateau at a slightly higher voltage of ∼1.3 V (and a shoulder at ∼1.9 V). The total discharge capacity is 828 mAh g^{-1} (∼7.6 mol of Li) and exactly coincides with that of the first charge capacity (Fig. 3a). This indicates that the electrochemical reaction is completely reversible and the capacity compares well with the value of 7.33 mol of Li expected from Eqs. (2) to (4). The second charge reaction is analogous to the first charge reaction but shows a slightly lesser capacity, 810 mAh g^{-1} (∼7.4 mol of Li). The voltage profiles of selected cycles up to 35 cycles are shown

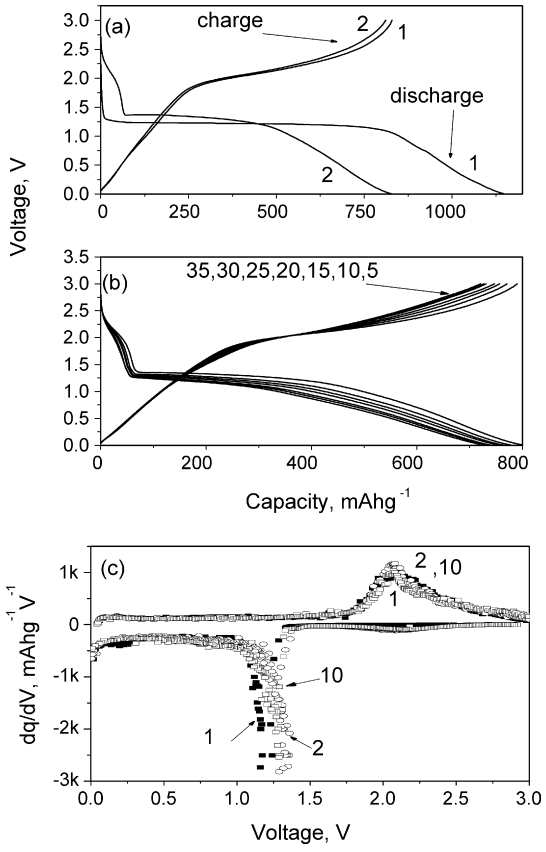

Fig. 3. The voltage vs. capacity profiles of nano-$CuCo_2O_4$ in the voltage range 0.005–3.0 V at 60 mA g^{-1} at room temperature. (a) The first and second discharge–charge cycles are shown. (b) The profiles of 5–35 cycles. Selected cycles are only shown for clarity. (c) The differential capacity (dq/dV) vs. voltage plots for the 1st, 2nd and 10th cycles extracted from the voltage-profiles of (a and b). The numbers indicate cycle number.

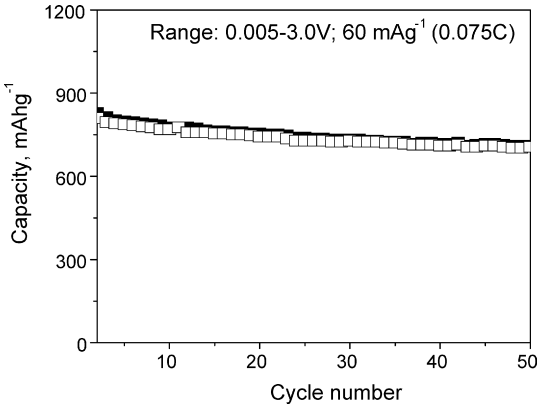

Fig. 4. Capacity vs. cycle number plot for nano-$CuCo_2O_4$ in the voltage range 0.005–3.0 V at current rate, 60 mA g^{-1}. Filled and open symbols correspond to discharge- and charge-capacities, respectively.

in Fig. 3b. These profiles are similar to the voltage profile of the 2nd cycle in all respects, which indicates good lithium recyclability after the first cycle. The gradually diminishing spread of the voltage profiles is indicative of continuous capacity fading upon cycling. To illustrate the galvanostatic cycling results in more detail, the capacity versus cycle number plot up to 50 cycles is shown in Fig. 4. As is quite evident, $CuCo_2O_4$ exhibits small capacity fading with an average capacity loss of 2 mAh g^{-1} per cycle, in the range of 2–50 cycles. Typical values of the discharge and charge capacities at the 20th cycle are 755 (±10) mAh g^{-1} (~6.9 mol of Li) and 745 (±10) mAh g^{-1} (~6.8 mol of Li), respectively. The coulombic efficiency increases during 2–15 cycles and stabilizes at ~98% between 20 and 50 cycles.

The cycling performance of nano-$CuCo_2O_4$ compares well with that of the iso-structural Co_3O_4 extensively investigated in the literature: For instance, Badway et al. [17] obtained high values, i.e., ~1000 mAh g^{-1}, that were stable up at least 70 cycles. On the other hand, Kang et al. [5] reported a reversible capacity of 700 mAh g^{-1}, of which 93.4% was retained after 100 cycles, whereas Zhao et al. [6] obtained a stable capacity, up to 50 cycles, of 740 mAh g^{-1}. Recently, Needham et al. [18] reported a capacity of over 800 mAh g^{-1}, stable up to 50 cycles, for the composite Co_3O_4–C, but they also found that pure Co_3O_4 which exhibited a second-cycle capacity of ~900 mAh g^{-1} could retain only 40% of the capacity after 35 cycles.

3.2.2. *Ex situ TEM*

Ex situ TEM studies were performed on fully-charged (3.0 V) $CuCo_2O_4$. The compound in the charged-state was recovered after 50 cycles and processed following the procedure described in Section 2. The HR-TEM image and SAED pattern are shown in Fig. 5a and b, respectively. Small-sized (3–6 nm), well-crystalline regions are seen to be embedded in an amorphous matrix (Fig. 5(a)). The double arrows marked with numbers (1–4) indicate some of the crystalline regions. Careful investigation of the d-spacings derived from the lattice fringes (1–4 in Fig. 5a) reveals that there are two phases, viz., CuO and Co_3O_4 (Table 1). The amorphous regions in Fig. 5a are comprised predominantly of Li_2O. The SAED pattern in Fig. 5b shows small bright spots that are overlapped by diffuse spots/rings, which are indicative of the nano-crystalline nature of the materials. The d-values calculated from the lattice image (Fig. 5a) and SAED pattern of Fig. 5b are listed in Table 1 and show fairly good agreement with the reported d-values of monoclinic CuO and cubic Co_3O_4. To re-confirm the Co_3O_4 formation, three different regions of the $CuCo_2O_4$-TEM sample were examined. In all the cases only Co_3O_4 was observed. Thus, the present study confirms formation of Co^{3+} (Co_3O_4) upon charging the active material up to 3 V. A similar observation of Co_3O_4 and ZnO formation has been found for nano-$ZnCo_2O_4$ [11]. Kang et al. [5] and Pralong et al. [19] also noted the re-formation of Co_3O_4 during their studies of the Co_3O_4–Li system. Interestingly, Yu et al. [7] also found Co_3O_4 in the charged-state of a CoO–Li_2O thin film composite anode. Therefore, we conclude that the nano-phases, formed on charging the composite electrode, are comprised of CuO and Co_3O_4.

3.2.3. *Reaction mechanism*

The voltage versus capacity profiles of $CuCo_2O_4$ bear a close resemblance to those of binary transition metal oxides MO (M = Co, Ni, Fe, Cu) [1,2] and ternary metal oxides $Ca_2Co_2O_5$ [9] and $ZnCo_2O_4$ [10,11] when they are cycled with Li. Hence, the reaction mechanism proposed in Eqs. (1)–(4) can be applied

Table 1
Comparison of the inter-planar spacings (*d*-values) derived from the HR-TEM lattice image (Fig. 5a) and SAED pattern (Fig. 5b) of the charged electrode of $CuCo_2O_4$ (3.0 V; after 50 cycles) with the reported data on CuO (monoclinic; JCPDS #80-1917) and Co_3O_4 (cubic; JCPDS #78-1969)

HR-TEM-image		SAED pattern	CuO *d*(Å) (*h k l*)	Co_3O_4 *d*(Å) (*h k l*)
Number	*d*(±0.03) Å	*d*(±0.03) Å		
1	2.48	2.52	2.5263 (0 0 2/$\bar{1}$ 1 1)	–
2	2.40	2.42	–	2.4377 (3 1 1)
3	2.05	2.03	1.9629 ($\bar{1}$ 1 2)	2.0212 (4 0 0)
4	1.87	1.85	1.8696 ($\bar{2}$ 0 2)	1.8548 (3 3 1)
–	–	1.54	1.5795 (2 0 2)	1.5559 (5 1 1)

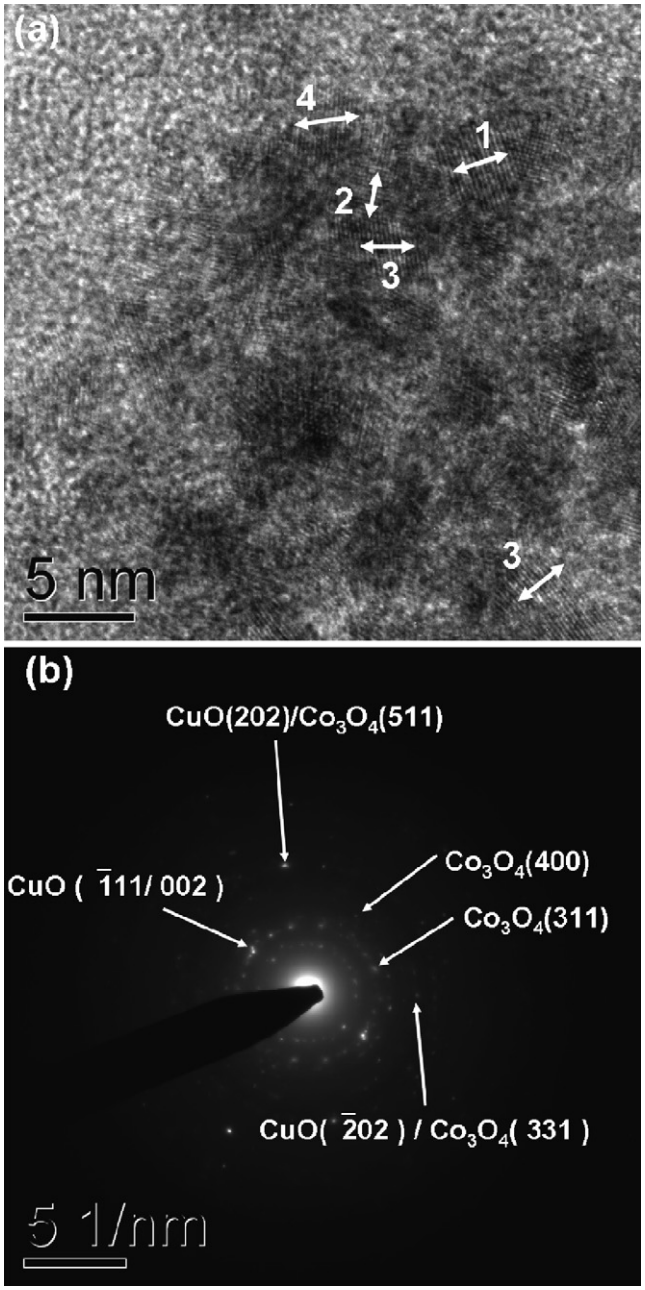

Fig. 5. Ex situ TEM of the charged electrode of $CuCo_2O_4$ (charged to 3.0 V after 50 cycles at 25 °C). (a) HR-TEM lattice image. The double arrows (↔) marked with numbers 1–4 indicate some of the nano-crystalline regions. The *d*-spacings calculated from the marked regions are given in Table 1. (b) The corresponding SAED pattern. The *d*-values derived from the pattern are given in Table 1.

to nano-$CuCo_2O_4$. The first discharge reaction is the irreversible structure–destruction process with the consumption of 8 mol of Li per mole of $CuCo_2O_4$ and the formation of electrochemically-active Co and Cu nano-particles in a matrix of Li_2O as per Eq. (1). The actual number of moles of Li (∼10.4) involved in the first discharge reaction is higher than the theoretically envisaged value by ∼2.4 mol of Li. This difference is attributable to a well-established cause, viz., the formation of a solid electrolyte interphase (SEI) at the electrode/electrolyte interface and the polymeric gel-type layer on the metal nano-particles [9–11,19]. The subsequent charge cycle is associated with the forward reaction of Eqs. (2)–(4) thereby releases ∼7.6 mol of Li (Figs. 3a and 4). This value is 0.27 mol of Li larger than the theoretical value of 7.33 mol of Li and possibly involves a contribution from the dissolution of the polymeric layer. From the second cycle onwards, cycling takes place as per the reversible reactions given by Eqs. (2)–(4).

The discharge voltage profiles (Fig. 3b and c) show that nano-Cu and Co metal particle formation occurs at ∼1.3 V whereas the charge-capacity is distributed over the entire charge cycle with an average charge potential, ∼2.1 V. This indirectly suggests that, due to the metal-ion and Li_2O matrix effect, the average reaction voltages involving Co (Eqs. (3) and (4)) and Cu (Eq. (2)) are almost the same. It must be mentioned here that there is no indication in the voltage-capacity profiles (Fig. 3) of Cu^+ formation (as Cu_2O) in the reversible reaction of Eq. (2), even though it must be occurring as an intermediate phase, viz., $Cu \leftrightarrow Cu^+ \leftrightarrow Cu^{2+}$.

3.2.4. Cyclic voltammetry

The galvanostatic cycling studies were complemented by cyclic voltammetry performed in the potential range 0.005–3.0 V versus Li at a sweep rate, of 58 μV s^{-1}. The first cycle commenced cathodically from the OCV to 0.005 V. The cyclic voltammograms (CV) shown in Fig. 6 bear strong resemblance to those of the differential capacity versus *V* plots given in Fig. 3c. Slight differences in the peak potentials in Figs. 3c and 6 can be attributed to differences in the mode of electrochemical cycling. The CV of the first discharge reaction has a pronounced peak at ∼0.95 V with an onset at ∼1.25 V. The charging curve (oxidation) is relatively smooth up to ∼1.7 V and has a broad peak at ∼2.1 V. The peak in the discharge cycle is attributable to the structure destruction of $CuCo_2O_4$ and the formation of Cu and Co nano-particles in an amorphous matrix of Li_2O (Eq. (1)). The broad peak around 2.0–2.3 V in the charge cycle can be

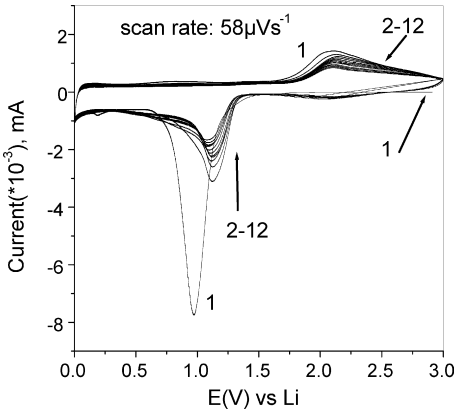

Fig. 6. Cyclic voltammograms of nano-$CuCo_2O_4$ in the potential range 0.005–3.0 V at a constant sweep rate, 58 $\mu V\,s^{-1}$ for the 1–12 cycles. Selected cycles are shown for clarity and numbers indicate the cycle number.

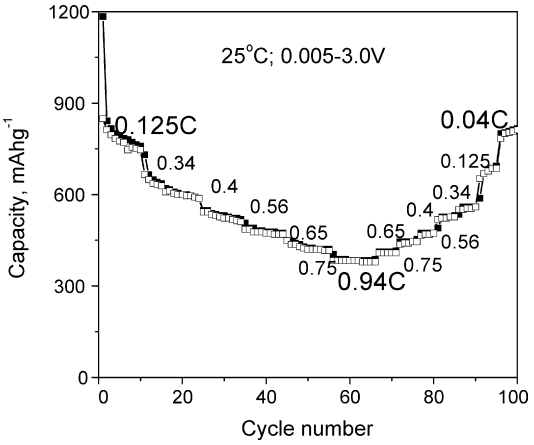

Fig. 7. Capacity vs. cycle number plot at various current rates of nano-$CuCo_2O_4$ to indicate the rate capability. The C values corresponding to different current rates are indicated, assuming $1C = 800\,mA\,g^{-1}$.

assigned to the oxidation of both Cu and Co metal nano-particles to the respective metal oxides (forward reactions of Eqs. (2)–(4). Further, the low intensity peak in the charge cycle is attributed to the capacity spread over the entire charge sweep.

The second discharge sweep comprises a peak at a relatively higher voltage, ~1.15 V in comparison to that of ~0.95 V observed in the first discharge curve. This indicates that the reaction mechanism with Li differs from the first discharge reaction and represents the formation of Co and Cu metal from the respective oxides, CuO/Co_3O_4, according to the backward reactions of Eqs. (2)–(4). The CVs of the subsequent 5th and 12th cycles resemble that of the 2nd cycle except for gradually diminishing peak intensities and a gradual shifting of the peak potentials to lower values, which thereby reflects the slow capacity fading upon cycling. In the case of binary oxides CoO and Cu_2O and ternary nano-$ZnCo_2O_4$, the average potential corresponding to CoO formation is ~2.1 V [1] and further oxidation of CoO to Co_3O_4 in nano-$ZnCo_2O_4$ occurs at ~2.4 V [11]. CuO formation upon charging also has been observed at ~2.5 V [12]. Thus, the broad symmetric anodic peak at ~2.1 V found in the present study on $CuCo_2O_4$ in the CV (Fig. 6) and in the differential capacity versus voltage curves (Fig. 3c), can be assigned to the formation of nano-CuO and nano-Co_3O_4 formation. The oxidation of CoO to Co_3O_4, in accordance with Eq. (4), is also supported by ex situ TEM data (Fig. 5 and Table 1) and the observed reversible capacity value (Fig. 3). Interestingly, the presence of a Co-oxide matrix is able to decrease the oxidation potential from 2.5 V in CuO [12] to ~2.1 V in nano-$CuCo_2O_4$.

Thus, on the basis of ex situ TEM, reversible capacity values and electrochemical behaviour (plateau potentials in galvanostatic cycling and peak positions in CV and differential capacity versus voltage curves), the conclusion can be drawn that, upon charging, the Cu- and Co-metal oxidize to CuO and Co_3O_4 and satisfy Eqs. (2)–(4).

3.2.5. Rate capability

The encouraging galvanostatic cycling behaviour, supported by CV studies, and the observed high and almost-stable capacity of $CuCo_2O_4$ encouraged a study of the rate capability using various current densities under ambient-temperature galvanostatic conditions in the voltage range 0.005–3.0 V. The specific current was increased in steps after every 10 cycles from 0.125 to 0.94C ($1C = 800\,mA\,g^{-1}$) and then decreased in steps up to 0.04C. The results in the form of capacity versus cycle number plot at different current rates are shown in Fig. 7. The capacity values decrease with increasing the current rate as can be expected. Thus, a capacity of 825 mAh g^{-1} at 0.125C decreases to 380 mAh g^{-1} upon increasing the current rate by 7.5 times. However, this value is higher than the theoretically achievable capacity value with the graphite anode and leads to the conclusion that reasonable capacity values are achievable with $CuCo_2O_4$ at good current rates. Upon decreasing the current rate from 0.94 to 0.04C through various steps, the capacity value started increasing and the recovery is ~79% of the value at 0.125C. When the current rate is decreased to ~0.04C (30 mA g^{-1}), a reversible capacity of 780 mAh g^{-1} (~7.1 mol of Li) is achieved at the end of 100 cycles. This value is close to that obtained with $CuCo_2O_4$ at 0.075C (60 mA g^{-1}) at the end of 50 cycles (Fig. 4). Therefore, the spinel nano-$CuCo_2O_4$ exhibits good rate-dependent characteristics.

4. Conclusions

Nano-phase $CuCo_2O_4$ has been synthesized by a low-temperature (~400 °C) urea combustion method and characterized by XRD, HR-TEM and SAED. The compound is almost a single phase except for a slight CuO impurity, and possesses a spinel structure and nano-particle morphology (particle size <20 nm). Galvanostatic cycling of $CuCo_2O_4$ at 60 mA g^{-1} in the voltage range 0.005–3.0 V exhibits a first charge capacity of 828 mAh g^{-1}. The irreversible capacity loss during the first discharge charge cycle is 28%. Typical discharge and charge capacity values at the 20th cycle are ~755 mAh g^{-1} (~6.9 mol of Li per mole of $CuCo_2O_4$) and ~745 mAh g^{-1} (~6.8 mol of Li), respectively. These values correspond to a coulombic efficiency of ~98% between the discharge and charge capacity. This value is retained for 20–50 cycles. The average discharge and charge reaction plateau potentials are ~1.2 and ~2.1 V, respectively. Cycling studies up to 50

cycles show almost stable cycling performance with a nominal capacity loss of 2 mAh g^{-1} per cycle between 2 and 50 cycles. Reversible cycling takes place by $Co \leftrightarrow CoO \leftrightarrow Co_3O_4$ and $Cu \leftrightarrow CuO$ redox reactions with Li_2O as given by Eqs. (2)–(4) aided by a polymeric gel-type layer formed during the initial discharge reaction. The observed plateau potentials in the voltage-capacity curves and cyclic voltammetry are consistent with the reaction mechanism proposed in Eqs. (2)–(4) and are well supported by ex situ TEM studies of the charged electrode. The lithium recyclability of nano-$CuCo_2O_4$ is comparable with that reported for iso-structural Co_3O_4 and $ZnCo_2O_4$.

References

[1] P. Poizot, S. Laruelle, S. Grugeon, L. Dupont, J.-M. Tarascon, Nature 407 (2000) 496.
[2] A.S. Arico, P. Bruce, B. Scrosati, J.-M. Tarascon, W.V. Schalkwijk, Nat. Mater. 4 (2005) 366.
[3] Z.-W. Fu, Y. Wang, Y. Zhang, Q.-Z. Qin, Solid State Ionics 170 (2004) 105.
[4] W.-Y. Li, L.-N. Xu, J. Chen, Adv. Funct. Mater. 15 (2005) 851.
[5] Y.-M. Kang, M.-S. Song, J.-H. Kim, H.-S. Kim, M.-S. Park, J.-Y. Lee, H.K. Liu, S.X. Dou, Electrochim. Acta 50 (2005) 3667.
[6] Z.W. Zhao, Z.P. Guo, H.K. Liu, J. Power Sources 147 (2005) 264.
[7] Y. Yu, C.H. Chen, J.-L. Shui, S. Xie, Angew. Chem. Int. Ed. 44 (2005) 7085.
[8] R. Alcantara, M. Jaraba, P. Lavela, J.L. Tirado, Chem. Mater. 14 (2002) 2847.
[9] N. Sharma, K.M. Shaju, G.V. Subba Rao, B.V.R. Chowdari, Electrochim. Acta 49 (2004) 1035.
[10] C. Al, M. Yin, C. Wang, J. Sun, J. Mater. Sci. 39 (2004) 1077.
[11] Y. Sharma, N. Sharma, G.V. Subba Rao, B.V.R. Chowdari, Adv. Funct. Mater., in press, doi:10.1002/adfm.200600997.
[12] X.P. Gao, J.L. Bao, G.L. Pan, H.Y. Zhu, P.X. Huang, F. Wu, D.Y. Song, J. Phy. Chem. B 108 (2004) 5547.
[13] M. Shimada, F. Kanamaru, M. Koizumi, N. Yamamoto, Mater. Res. Bull. 10 (1975) 733.
[14] K. Petrov, T. Karamaneva, S. Angelov, D. Mehandjiew, Mater. Res. Bull. 18 (1983) 637.
[15] A.C. Tavares, M.A.M. Cartaxo, M.I.D.S. Pereira, F.M. Costa, J. Solid State Electrochem. 5 (2001) 57.
[16] K.C. Patil, S.T. Aruna, S. Ekambaram, Curr. Opin. Solid State Mater. Sci. 2 (1997) 158.
[17] F. Badway, I. Plitz, S. Grugeon, S. Laruelle, M. Dolle, A.S. Gozdz, J.-M. Tarascon, Electrochem. Solid-State Lett. 5 (2002) A115.
[18] S.A. Needham, G.X. Wang, K. Konstantinov, Y. Tournayre, Z. Lao, H.K. Liu, Electrochem. Solid-State Lett. 9 (2006) A315.
[19] V. Pralong, J.B. Leriche, B. Beaudoin, E. Naudin, M. Morcrette, J.-M. Tarascon, Solid State Ionics 166 (2004) 295.